Synthesis, Exchange Reactions, and Metallacycle Formation in Osmium(II) Imido Systems: Formation and Cleavage of Os–N Bonds

Richard I. Michelman, Robert G. Bergman,* and Richard A. Andersen*

Department of Chemistry, University of California, Berkeley, California 94720

Received April 2, 1993

Monomeric, low oxidation state, osmium–imido compounds (η^6-arene)OsN-*t*-Bu (arene = *p*-cymene (**2a**) and C_6Me_6 (**2b**)) have been synthesized from [(η^6-arene)$OsCl_2$] (arene = *p*-cymene (**1a**) and C_6Me_6 (**1b**)) and 4 equiv of LiNH-*t*-Bu in THF. Further characterization of complex **2a** was obtained by ^{15}N NMR spectrometry on the corresponding ^{15}N-labeled species (**2a**-^{15}N). An X-ray crystal structure of complex **2b** showed a short Os–N distance (1.737(7) Å) and a nearly linear Os–N–C angle (174.1(7)°) consistent with osmium to nitrogen multiple bonding. The imide **2a** undergoes exchange reactions with $H_2N(2,6\text{-}Me_2C_6H_3)$ to yield CymOsN(2,6-$Me_2C_6H_3$) (**3**) with liberation of H_2N-*t*-Bu. A mechanistic study of this imide/amine exchange showed that the reaction rate is first order in **2a** and first order in entering amine, and that $k_H/k_D = 5.7$ when $D_2N(2,6\text{-}Me_2C_6H_3)$ is used. These data suggest that the reaction proceeds through a bis(amide) intermediate and that N–H bond cleavage is involved in the rate determining step. Although the bis(amide) complex was not observed by ^1H NMR spectroscopy, the analogous chelated complex CymOs[1,2-$(NH)_2C_6H_4$] (**5**) was isolated from the reaction of **1a** with 1,2-$(H_2N)_2C_6H_4$. Imide **3** can also be prepared from **1a** and 4.2 equiv of LiNH(2,6-$Me_2C_6H_3$). The imide CymOsN[2,6-(*i*-Pr)$_2C_6H_3$] (**4**) can be prepared using LiNH[2,6-(*i*-Pr)$_2C_6H_3$]. Compound **2a** undergoes cycloaddition reactions with *t*-BuNCO and RN_3 to give the ureylene complex CymOs[(N-*t*-Bu)$_2$CO] (**6**) (Cym = η^6-*p*-cymene) and tetrazene compounds CymOs[N(*t*-Bu)N=NN(R)] (R = Ph (**7**), $SiMe_3$ (**8**), CPh_3 (**9**), *t*-Bu (**10**)). An X-ray crystal structure of phenyl derivative **7** showed a planar OsN_4 core with the isopropyl group of the *p*-cymene ligand tilted away from the large *tert*-butyl group. Variable temperature NMR studies with **7–9** suggest that the solution conformation of these complexes is dependent on the size of the substituent R.

Introduction

Transition metal imido complexes have been postulated to be important intermediates in a number of industrial processes.[1–4] Other applications have emerged that use imido complexes as precursors to solid state materials,[5] in homogeneous catalysis,[6] and in living polymerization.[7,8] Many of the complexes involved rely on a strong metal–nitrogen bond and are derived from the center of the transition series (V–Mn and their second and third row congeners).[9,10]

Recently, the synthesis of the monomeric, low oxidation state, imido complex Cp*IrN-*t*-Bu (Cp* = η^5-$C_5(CH_3)_5$) has been achieved.[11] Despite its surprising stability[12] this unusual species undergoes reactions that are unexpected, including cycloadditions, coupling–trapping reactions, and nucleophilic additions. The isolobal and isoelectronic compounds (η^6-arene)OsNR prepared here offer an expanded view of the range of chemistry available to late transition metal imides.[13] They differ from the complexes [(η^6-*p*-cymene)RuNR]$_2$ in both nuclearity and reactivity.[14,15]

Results

Synthesis and Characterization of Osmium Imido Complexes. Simple metathesis reactions were employed in the one step preparation of the monomeric compounds (η^6-arene)OsNR (eq 1).

$$\underset{\mathbf{1}}{[(\eta^6\text{-arene})OsCl_2]_2} + 4LiNHR \xrightarrow{THF} 2\underset{\mathbf{2-4}}{(\eta^6\text{-arene})Os{\equiv}NR} \quad (1)$$

R = *t*-Bu; arene = Cym (**2a**), C_6Me_6 (**2b**)
R = 2,6-$Me_2C_6H_3$; arene = Cym (**3**)
R = 2,6-(*i*-Pr)$_2C_6H_3$; arene = Cym (**4**)

Treatment of $[CymOsCl_2]_2$ (Cym = η^6-*p*-cymene) (**1a**) or [(η^6-C_6Me_6)$OsCl_2$]$_2$ (**1b**)[16] with 4 equiv of LiNH-*t*-Bu in tetrahydrofuran (THF) provided the imido compounds (η^6-arene)OsN-*t*-Bu (arene = Cym (**2a**), C_6Me_6 (**2b**)) as yellow crystals from pentane in 85–95% yield. The

(1) Chan, D. M.-T.; Fultz, W. C.; Nugent, W. A.; Roe, D. C.; Tulip, T. H. *J. Am. Chem. Soc.* **1985**, *107*, 251.
(2) Nugent, W. A. *Inorg. Chem.* **1983**, *22*, 965 and references therein.
(3) Burrington, J. D.; Grasselli, R. K. *J. Catal.* **1979**, *59*, 79.
(4) Keulks, G. W.; Krenzke, L. D.; Noterman, T. M. *Adv. Catal.* **1978**, *27*, 183.
(5) Winter, C. H.; Sheridan, P. H.; Lewkebandara, T. S.; Heeg, M. J.; Proscia, J. W. *J. Am. Chem. Soc.* **1992**, *114*, 1095.
(6) Herranz, E.; Sharpless, K. B. *J. Org. Chem.* **1978**, *43*, 2544.
(7) Schrock, R. R.; Murdzek, J. S.; Bazan, G.; Robbins, J.; DiMare, M. *J. Am. Chem. Soc.* **1990**, *112*, 3875.
(8) Murdzek, J. S.; Schrock, R. R. *Organometallics* **1987**, *6*, 1373.
(9) Nugent, W. A.; Mayer, J. M. *Metal Ligand Multiple Bonds*; John Wiley and Sons: New York, 1988.
(10) Nugent, W. A.; Haymore, B. L. *Coord. Chem. Rev.* **1980**, *31*, 123.
(11) Glueck, D. S.; Wu, J.; Hollander, F. W.; Bergman, R. G. *J. Am. Chem. Soc.* **1991**, *113*, 2041.
(12) Mayer, J. M. *Comments Inorg. Chem.* **1988**, *8*, 125.
(13) For a review of the organometallic chemistry of (arene)Os complexes, see: LeBozec, H.; Touchard, D.; Dixneuf, P. *Adv. Organomet. Chem.* **1989**, *29*, 163.
(14) Michelman, R. I. Ph.D. Dissertation, University of California, Berkeley, CA, 1993.
(15) A portion of the work described here has been reported in preliminary form: Michelman, R. I.; Andersen, R. A.; Bergman, R. G. *J. Am. Chem. Soc.* **1991**, *113*, 5100.
(16) Kiel, W. A.; Ball, R. G.; Graham, W. A. G. *J. Organomet. Chem.* **1990**, *383*, 481.

0276-7333/93/2312-2741$04.00/0

metathesis reactions also proceeded smoothly with LiNH(2,6-$R_2C_6H_3$) (R = Me, *i*-Pr) and **1a** to give the purple arylimido complexes CymOsN(2,6-$Me_2C_6H_3$) (**3**) and CymOsN[2,6-(*i*-Pr)$_2C_6H_3$] (**4**). Although imides **2** and **3** are readily crystallized from pentane, isolation of **4** in crystalline form was more difficult due to its high solubility.

As was observed for Cp*IrN-*t*-Bu,[11] the *tert*-butyl signals for **2a** and **2b** appear as a three line pattern of intensity 1:1:1 (J = 1.5 Hz) in the ^{1}H NMR spectrum due to coupling to ^{14}N (I = 1). Compounds with axially symmetric electron density at the nitrogen nucleus (i.e. other imides and alkyl isocyanides) frequently show similar coupling. Observation of this phenomenon suggests a linear X–N–C linkage.[9] The labeled imido complex CymOs^{15}N-*t*-Bu (**2a**-^{15}N), prepared from **1a** and Li^{15}NH-*t*-Bu,[11] shows a doublet for the *tert*-butyl resonance (J = 2.4 Hz) in the ^{1}H NMR spectrum due to coupling to ^{15}N (I = $^1/_2$). The observed coupling constants are consistent with the expression $J(^{14}N–X) = -0.713[J(^{15}N–X)]$, where 0.713 is the magnetogyric ratio of the nitrogen isotopes.[17] The $^{13}C\{^1H\}$ NMR spectrum of **2a**-^{15}N shows coupling between ^{15}N and the *tert*-butyl group (both the primary and quaternary carbons with $J \cong 0.6$ Hz in each case) as well as coupling to the arene ring carbons ($J \cong 0.8$ Hz). The doublets in the $^{13}C\{^1H\}$ NMR spectrum were seen only upon zerofilling on the FID. These values are consistent with other $J(^{15}N–^{13}C)$ measurements.[18] This phenomenon is not observed in the $^{13}C\{^1H\}$ NMR spectrum of **2a** since the coupling constants should be on the order of the line width, as predicted by the above formula. Compound **2a**-^{15}N displays a broad singlet at δ –65.0 (with respect to CH_3NO_2 in C_6D_6) in the $^{15}N\{^1H\}$ NMR spectrum, but no $J(^{187}Os–^{15}N)$ was observed. A variable temperature ^{1}H NMR study of **2a** has shown that the aromatic *p*-cymene proton resonances appear as a singlet in the room temperature ^{1}H NMR spectrum, which splits into two doublets at both higher and lower temperatures, as expected for an AA'BB' spectrum.

Although the NMR spectra of arylimide **3** are not unusual, the tertiary methine protons and carbon resonances for the isopropyl groups on the arylimide ligand of **4** are broad at room temperature. A C–H correlated spectrum showed a cross-peak linking these ^{1}H and $^{13}C\{^1H\}$ NMR resonances. The ^{1}H NMR signal sharpens into a septet at 40 °C while no other line shape changes are observed. Upon cooling a toluene-d_8 solution of **4** in the NMR probe, the CH resonance for the aryl isopropyl groups coalesces at –4 °C and reemerges as two broad peaks at –9 °C. The corresponding methyl doublet also broadens and becomes two peaks at –13 °C, which appear as doublets at –58 °C. This variable temperature behavior also affects the metal center such that at –58 °C, the resonances for the aromatic *p*-cymene protons and the methyl protons of the isopropyl group on the *p*-cymene ligand appear as four doublets and two doublets, respectively. These temperature dependent phenomena are presumably due to a combination of conformational interconversions that we have not analyzed in detail. A study in another (η^6-arene)Os system with bulky ligands has shown that ring tilting can be hindered and rotation can be restricted.[19]

Observation of the ^3J(N—H) coupling constant mentioned above requires effective cylindrical symmetry and therefore suggests strongly that the osmium imide is a monomer. Further support for the monomeric nature of imido complexes **2** was obtained from infrared and mass spectra. Infrared stretching absorptions characteristic of monomeric imido ligands[9] were observed at 1250 cm^{-1} for both **2a** and **2b**. This assignment was confirmed by the 15-cm^{-1} shift of this absorption to 1235 cm^{-1} for **2a**-^{15}N.[20] A shift to 1211 cm^{-1} on ^{15}N substitution is predicted by a simple harmonic oscillator calculation. The observed bands may therefore be due to a combination of M=N and N—C stretches, as has been suggested for other monomeric imido complexes[9,11,21] and studied in detail by Shapley and co-workers.[22] The arylimido complexes **3** and **4** show these strong bands at 1220 and 1189 cm^{-1}, respectively. The electron impact mass spectra for **2a** and **2a**-^{15}N display [M]$^+$ at *m/e* 397 and 398 (^{192}Os), respectively. The spectrum for xylylimide **3**, however, shows a single parent ion approximately consistent with a dimeric structure (*m/e* 889; *m/e* 890 expected), but the isotope peaks were not observed. A similar result had been obtained for Cp*IrN(2,6-$Me_2C_6H_3$), which was shown crystallographically to be monomeric.[11] In the absence of more information, we assume that all of the osmium imides (**2–4**) are monomeric.

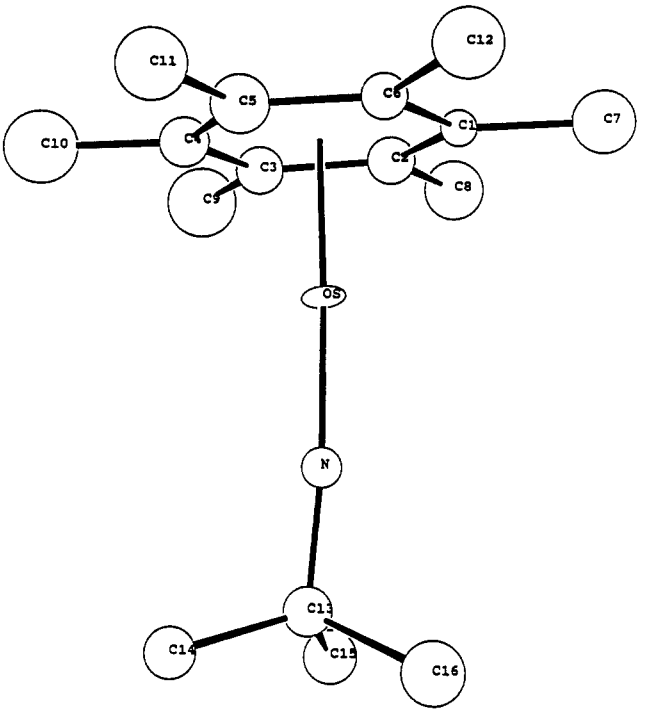

Figure 1. ORTEP diagram of (C_6Me_6)OsN-*t*-Bu (**2b**).

Crystal Structure of *tert*-Butylimido Complex 2b. The monomeric nature of **2b** was confirmed by an X-ray diffraction study performed on a single yellow crystal obtained from a heptane solution cooled to –40 °C. An ORTEP diagram is provided in Figure 1. Compound **2b** adopts a "pogo-stick" geometry similar to that observed for Cp*IrN-*t*-Bu. The nearly linear Os–N–C angle of 174.1(7)° and the short Os–N bond distance of 1.737(7) Å are consistent with Os–N multiple bonding.[9] Table I contains a list of the bond lengths and angles.

(17) Gordon, A. J.; Ford, R. A. *The Chemist's Companion*; Wiley-Interscience: New York, 1971; p 229.
(18) Levy, G. C.; Lichter, R. L. *Nitrogen-15 Nuclear Magnetic Resonance Spectroscopy*; John Wiley and Sons: New York, 1979.
(19) Hu, X.; Duchowski, J.; Pomeroy, R. K. *J. Chem. Soc., Chem. Commun.* **1988**, 362.
(20) Osborne, J. H.; Trogler, W. C. *Inorg. Chem.* **1985**, *24*, 3098.
(21) Glassman, T. E.; Vale, M. G.; Schrock, R. R. *Organometallics* **1991**, *10*, 4046.
(22) Marshman, R. W.; Shapley, P. A. *J. Am. Chem. Soc.* **1990**, *112*, 8369.

Table I. Intramolecular Bond Distances (Å) and Angles (deg) for 2b

intramolecular distance		intramolecular angle	
Os–N	1.737(7)	N–Os–cent[a]	177.07(24)
Os–C1	2.266(9)	Os–N–C13	174.1(7)
Os–C2	2.251(10)	N–C13–C14	109.5(8)
Os–C3	2.232(10)	N–C13–C15	109.0(8)
Os–C4	2.212(10)	N–C13–C16	105.4(8)
Os–C5	2.219(11)	C14–C13–C15	114.4(9)
Os–C6	2.239(10)	C14–C13–C16	110.1(8)
Os–cent[a]	1.729(1)	C15–C13–C16	108.1(8)
N–C13	1.436(12)	C2–C1–C6	117.8(8)
C13–C14	1.511(14)	C2–C1–C7	120.3(9)
C13–C15	1.499(14)	C6–C1–C7	121.9(9)
C13–C16	1.625(15)	C1–C2–C3	122.4(9)
		C1–C2–C8	121.4(9)
C1–C2	1.399(13)	C3–C2–C8	116.1(9)
C1–C6	1.449(13)	C2–C3–C4	117.7(9)
C1–C7	1.509(14)	C2–C3–C9	122.6(10)
C2–C3	1.444(14)	C4–C3–C9	119.7(10)
C2–C8	1.522(15)	C3–C4–C5	120.8(10)
C3–C4	1.430(14)	C3–C4–C10	118.2(10)
C3–C9	1.499(17)	C5–C4–C10	121.0(10)
C4–C5	1.369(14)	C4–C5–C6	121.7(10)
C4–C10	1.509(17)	C4–C5–C11	122.6(10)
C5–C6	1.425(14)	C6–C5–C11	115.7(10)
C5–C11	1.535(16)	C1–C6–C5	119.5(9)
C6–C12	1.542(15)	C1–C6–C12	117.4(9)
		C5–C6–C12	122.9(9)

[a] cent = centroid of the benzene ring.

Imide/Amine Exchange Reaction and Kinetics. *tert*-Butylimide **2a** was easily converted to arylimide CymOsN(2,6-$Me_2C_6H_3$) (**3**) by amine exchange. Addition of 3.4 equiv of $H_2N(2,6\text{-}Me_2C_6H_3)$ to a benzene solution of **2a** resulted in complete conversion to **3** after 2 h at room temperature (eq 2). Analysis of the volatile materials

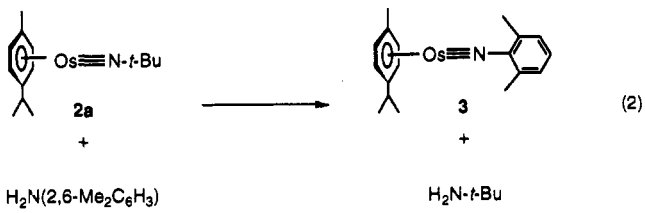

(2)

by ^1H NMR spectrometry showed 1 equiv of free *t*-$BuNH_2$. No back-reaction was observed when 6 equiv of H_2N-*t*-Bu and CymOsN(2,6-$Me_2C_6H_3$) were mixed in C_6D_6. The related proton transfer reaction between **2a** and the more hindered amine, $H_2N[2,6\text{-}(i\text{-}Pr)_2C_6H_3]$, did not occur to give **4** after heating a reaction solution at 45 °C for 4 days, as shown by ^1H NMR spectroscopy. Treatment of **2a** with 1 equiv of either $MeNH_2$ or NH_3 gave complex mixtures, as determined by their ^1H NMR spectra.

The conversion of CymOsN-*t*-Bu (**2a**) and $H_2N(2,6\text{-}Me_2C_6H_3)$ to H_2N-*t*-Bu and CymOsN(2,6-$Me_2C_6H_3$) (**3**) was investigated further in a kinetic study. Using UV–visible spectroscopy, the reaction rate was measured in toluene at 25 °C. The appearance of product was monitored by its absorbance at 514 nm over at least 3 half-lives. Runs were performed under pseudo-first-order conditions over an amine concentration range from 1.94 × 10^{-2} to 9.83 × 10^{-2} M using a **2a** concentration of 9.94 × 10^{-4} M. The large excess of amine assured that its concentration would remain essentially constant throughout each individual run. Plots of absorbance vs time were fit to an increasing logarithmic function ($\ln[A_\infty/(A_\infty - A)]$ vs time), which resulted in straight lines. Values for the rate constants were extracted as the slopes of these lines. These straight lines indicate that the reaction follows a first-order dependence on the concentration of **2a**. Table II contains the observed rate constants. A plot of $H_2N(2,6\text{-}Me_2C_6H_3)$ concentration vs the rate constant for product formation (k_{obs}) was linear (Figure 2), indicating that the reaction is also first-order in amine. Individual runs showed good reproducibility, as demonstrated by the multiple points for the concentration of amine at 3.88 × 10^{-2} and 6.29 × 10^{-2} M. The same methods were employed using $D_2N(2,6\text{-}Me_2C_6H_3)$ (Table III). For experiments at 3.9 × 10^{-2} M amine concentration, a deuterium isotope effect k^H_{obs}/k^D_{obs} of 5.7 was obtained.

No bis(amide) intermediate was observed in the imide/amine exchange reaction by ^1H NMR spectroscopy. In order to assess the stability of such an intermediate, the *tert*-butyl complex **2a** was treated with the diamine 1,2-$(H_2N)_2C_6H_4$ (Scheme I). The chelating bis(amide) complex CymOs[1,2-$(NH)_2C_6H_4$] (**5**) was isolated from this reaction as a yellow-orange precipitate from toluene at −40 °C. The N–H resonance is observed in the ^1H NMR spectrum at δ 8.68, and the corresponding stretching frequency appears in the IR spectrum at 3332 cm^{-1}.

Table II. Rate Data[a] for the Reaction of *tert*-Butylimide 2a and $H_2N(2,6\text{-}Me_2C_6H_3)$ in Toluene at 25 ± 1 °C

[**2a**] (M)	$[H_2N(2,6\text{-}Me_2C_6H_3)]$ (M)	k (s^{-1})
9.94 × 10^{-4}	1.94 × 10^{-2}	1.10 × 10^{-3}
	3.14 × 10^{-2}	2.20 × 10^{-3}
	3.88 × 10^{-2}	2.16 × 10^{-3}
	3.88 × 10^{-2}	2.27 × 10^{-3}
	6.29 × 10^{-2}	3.92 × 10^{-3}
	6.29 × 10^{-2}	4.06 × 10^{-3}
	7.74 × 10^{-2}	4.69 × 10^{-3}
	9.83 × 10^{-2}	5.71 × 10^{-3}

[a] Calculated standard deviation varied from ±0.02 to ±0.18 × 10^{-3} s^{-1}. Based on the reproducibility of the results from the points at 3.88 and 6.29 × 10^{-3} M, we estimate the random error to be ±6.3 × 10^{-5} s^{-1}.

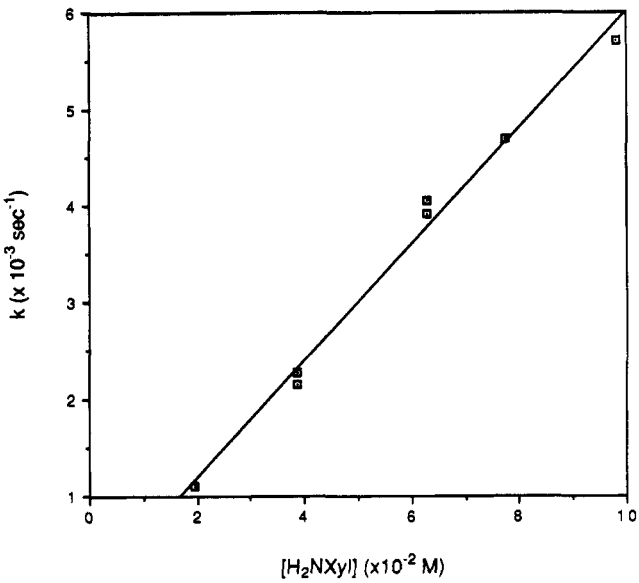

Figure 2. Plot of concentration vs rate constant for the amine/imide exchange reaction.

Table III. Rate Data for the Reaction of *tert*-Butylimide 2a and $D_2N(2,6\text{-}Me_2C_6H_3)$ in Toluene at 25 ± 1 °C

[**2a**] (M)	$[D_2N(2,6\text{-}Me_2C_6H_3)]$ (M)	k (s^{-1})
9.94 × 10^{-4}	3.89 × 10^{-2}	3.66 × 10^{-4}
	3.89 × 10^{-2}	3.79 × 10^{-4}
	3.89 × 10^{-2}	4.21 × 10^{-4}
av for D	3.89 × 10^{-2}	(3.89 ± 0.23) × 10^{-4}
av for H (from Table II)	3.88 × 10^{-2}	(2.21 ± 0.06) × 10^{-3}

Scheme I. Reaction of (η^6-*p*-Cymene)OsN-*t*-Bu (2a) with a Chelating Diamine

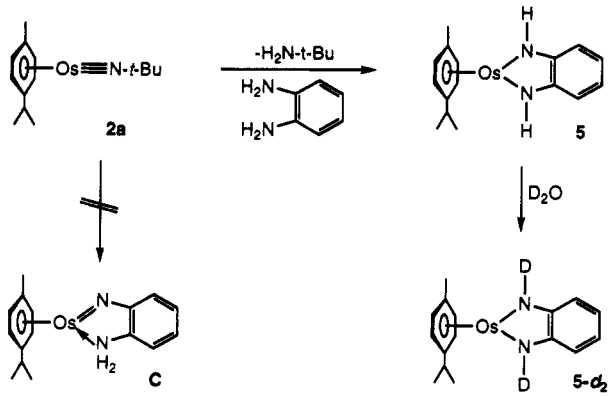

The deuterated chelating bis(amide) complex CymOs-[1,2-$(ND)_2C_6H_4$] (**5**-d_2) was prepared by treating a C_6D_6 solution of **5** with D_2O (Scheme I). The ^1H NMR spectrum of the product **5**-d_2 displayed no resonance at δ 8.68 and an N–D stretch appeared in the IR spectrum at 2474 cm^{-1}. This reduction in stretching frequency is close to the value of 2433 cm^{-1} predicted from a simple harmonic oscillator calculation.

Reaction of Imido Compound 2a with Isocyanates and Azides. Compound **2a** reacted with the heterocumulene *t*-BuNCO when heated at 45 °C for 36 h to give the blue-green ureylene metallacycle **6** (eq 3).[23,24] Complex

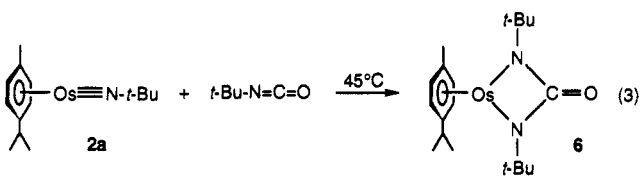

6 readily sublimes at 60 °C/80 mTorr and exhibits $[M]^+$ at *m/e* 496 in the electron-impact mass spectrum. The carbonyl carbon appears in the $^{13}C\{^1H\}$ NMR spectrum at δ 174.4, and an IR absorption due to the CO stretch is observed at 1656 cm^{-1}. Carbonyl absorptions for other monomeric ureylene complexes range from 1608 to 1698 cm^{-1}.[23] The 18-electron ruthenium complex CymRu-$(PMe_3)[(N\text{-}p\text{-tol})_2CO]$ shows this band at 1608 cm^{-1}.[14] A dimeric nitrogen bridged structure for **6** is unlikely since such a structure would exhibit diastereotopic isopropyl methyl groups and inequivalent aromatic proton signals in the ^1H and $^{13}C\{^1H\}$ NMR spectra, as well as two different types of *tert*-butyl resonances. The event that the resonances are accidentally degenerate or the molecule is fluxional is unlikely. The spectra of the crystallographically characterized dimer $\{(p\text{-cymene})Ru[(N\text{-}p\text{-tol})_2CO]\}_2$ show these spectral features,[14] so their absence in the osmium case provides additional support for the monomeric structure.

Treatment of **2a** with organic azides provided the yellow tetrazene compounds CymOs[N(*t*-Bu)N=NN(R)] (R = Ph (**7**), $SiMe_3$ (**8**), CPh_3 (**9**), *t*-Bu (**10**)) (Scheme II). The $SiMe_3$ (**8**) and *t*-Bu (**10**) metallacycles were very soluble in pentane and were therefore best purified by column chromatography. Compounds **7–10** are all somewhat thermally sensitive, and so they were stored at −40 °C. However, they could be manipulated in the absence of air and moisture for several hours at room temperature with little decomposition. The CPh_3 derivative **9** was the least stable, and satisfactory elemental analysis could not be obtained on this complex despite repeated attempts.

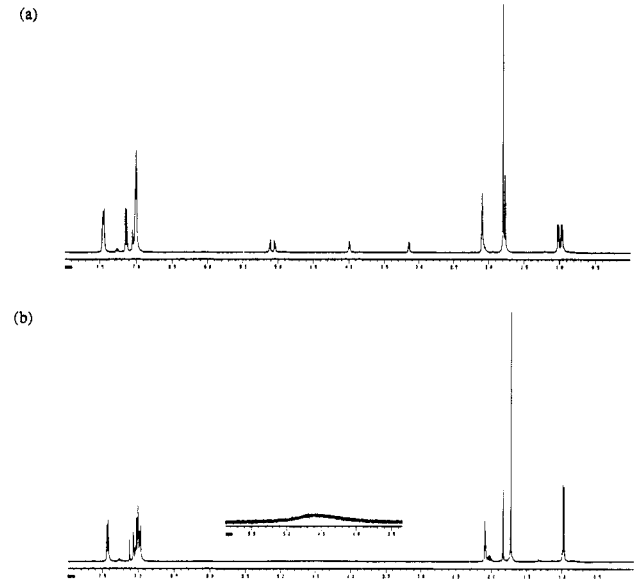

Figure 3. ^1H NMR spectra of tetrazene derivative **9** in toluene-d_8: (a) −21 °C; (b) 89 °C.

Scheme II. Reaction of *t*-Bu Imido Complex 2a with Organic Azides

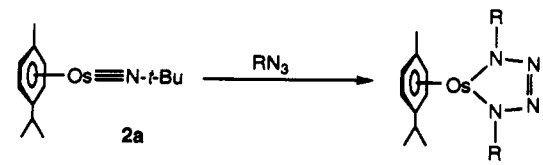

7, R = Ph; **8**, R = $SiMe_3$, **9**, R = CPh_3; **10**, R = t-Bu

The variable temperature ^1H NMR data for these compounds were dependent on the substituent on the azide. Although phenyl tetrazene complex **7** shows sharp resonances at room temperature, there is significant broadening of the resonances for the aromatic protons on the *p*-cymene and the methyl protons of the isopropyl group at lower temperatures. At −70 °C the methyl groups appear as two broad resonances and the two aromatic *p*-cymene resonances are broadened also. Complete resolution was not obtained with further cooling to −92 °C. The larger $SiMe_3$ substituent of **8** gave sharper resonances at lower temperatures. All resonances were sharp at 44 °C, but the aromatic proton resonances collapsed to two broad resonances at 21 °C. By −58 °C the ^1H NMR spectrum showed four doublets due to the aromatic protons and two overlapping doublets for the isopropyl methyl groups. A $^{13}C\{^1H\}$ NMR spectrum at this temperature displayed all the peaks expected for a decoalesced spectrum, while at room temperature it did not show resonances for the tertiary aromatic carbons. The CPh_3 derivative **9** displayed well resolved resonances demonstrating asymmetry at −21 °C in the ^1H NMR spectrum, including aromatic *p*-cymene C–H doublets shifted as far upfield as δ 3.14 and 3.99 (Figure 3a). The 21 °C spectrum showed significant broadening, but at 40 °C the resonances for the methyl protons of the isopropyl group averaged to one doublet. Unfortunately, the ring C–H resonances became extremely broad at 60 °C and only appeared as a single broad resonance at 89 °C (Figure

(23) For a review of transition metal isocyanate chemistry, see: Braunstein, P.; Noble, D. *Chem. Rev.* **1989**, *89*, 1927.

(24) For additional information on transition metal isocyanate chemistry, see: Cenini, S.; LaMonica, G. *Inorg. Chim. Acta* **1976**, *18*, 279.

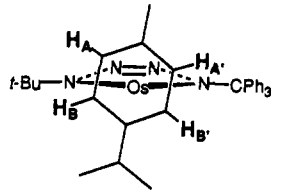

Figure 4. Conformational projection of **9**.

Table IV. Selected Cross-Peaks for Aromatic *p*-Cymene Resonances in the 2D-NOESY of 9 (−21 °C)

proton (from Figure 3)	^{1}H NMR (δ)	cross-peaks
Cym-H_B	5.11	Cym-H_A, *t*-Bu
Cym-H_A	5.04	Cym-H_B, *t*-Bu, Me
Cym-$H_{B'}$	3.99	Cym-$H_{A'}$, CPh_3
Cym-$H_{A'}$	3.14	Cym-$H_{B'}$, CPh_3, Me

3b). Finally, the symmetrical bis(*tert*-butyl) derivative **10** showed no line shape changes over a range of +20 to −85 °C.

2D-NOESY Analysis of Tetrazene Derivatives 8 and 9. In order to assign the resonances in the variable temperature NMR spectra, 2D-NOESY experiments were conducted on the $SiMe_3$ (**8**) and CPh_3 (**9**) derivatives. For the room temperature 2D spectrum of **8**, cross-peaks were observed between the aromatic proton resonances and the resonances for both $SiMe_3$ and *t*-Bu. This suggests the structure drawn for **8** below and in Scheme II, rather than

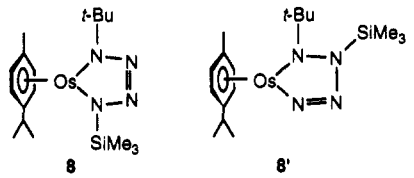

the alternative structure **8′** where a $SiMe_3$-*t*-Bu cross-peak should have been observed. The 2D-experiment also allowed us to assign the aromatic proton resonances on the *p*-cymene ligand. The more upfield resonance (δ 5.17) corresponds to the protons near the methyl group, while the resonance at δ 5.21 is due to the protons that are closer to the isopropyl group. Unfortunately, nothing was learned about the fluxional process or the lowest energy *p*-cymene ring conformation from this experiment.

The 2D-NOESY experiment on **9** at −21 °C was conducted in the hope that the unusual chemical shifts of the aromatic *p*-cymene resonances (δ 3.99 and 3.14) could be explained, or at least shown to belong to the aromatic ring. At this temperature in the ^{1}H NMR spectrum all resonances were observed without broadening. Cross-peak correlations are displayed in Table IV. Interestingly, no cross-peaks were seen to the isopropyl group. These data support the low temperature conformation shown in Figure 4. If there is slow *p*-cymene ring rotation, or rocking, about the pseudo-C_6 axis of the Os–Cym_{center} bond on the NMR time scale, all four aromatic protons (A, A′, B, B′) will have different chemical shifts, as is observed.

Molecular Structure of Phenyltetrazene Complex 7. An X-ray diffraction study was performed on a yellow single crystal of **7** obtained from a pentane solution cooled to −40 °C. Two ORTEP views of the structure are provided in Figure 5. The solid state structure confirmed the essential features of the N_4 ligand conformation inferred from the NOESY experiments. The most striking feature is the planar OsN_4 ring, whose largest deviation from the least-squares plane is only 0.032 Å. The quaternary

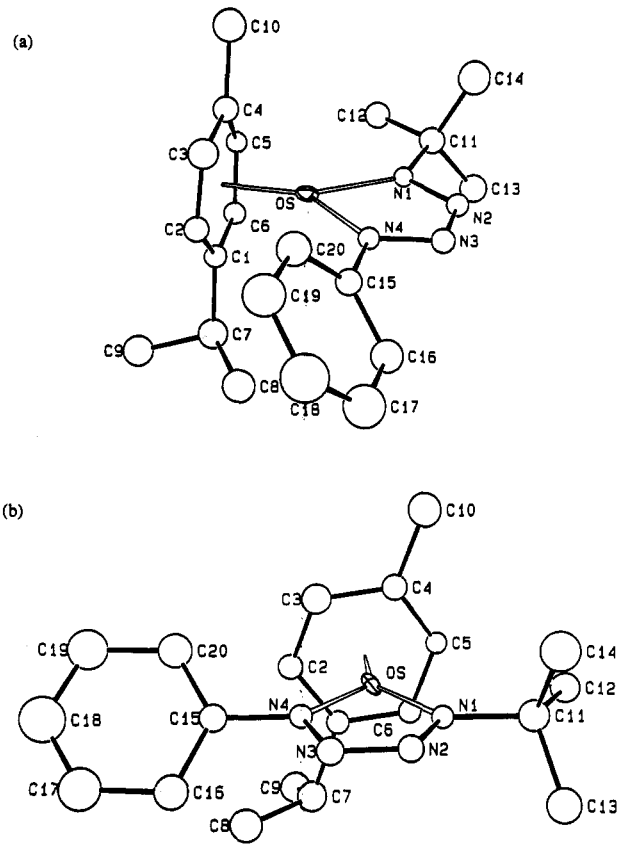

Figure 5. ORTEP diagrams of phenyl tetrazene derivative **7**.

carbons on both the *tert*-butyl and phenyl groups also lie in this plane. The Os–N distances are shorter to N–Ph (1.942(12) Å) than to N–*t*-Bu (1.977(13) Å), though not significantly so since both distances are equal to within 3σ, and the *p*-cymene ligand is tilted slightly toward the phenyl group (*p*-Cym_{center}–Os–N_{Ph} angle = 138.7°; *p*-Cym_{center}–Os–$N_{t\text{-}Bu}$ angle = 146.6°). The N–N bond distances are shortest between the unsubstituted nitrogen atoms (1.286(16) Å) and somewhat longer between the others (1.351(17) and 1.365(16) Å). These are normal bond distances for complexes of this type.[25] In contrast to the conformation proposed above for the CPh_3 derivative **9** (Figure 4), the isopropyl group on the *p*-cymene ligand points away from the larger *tert*-butyl substituent and toward the phenyl group (Figure 5b). Table V contains a list of the bond lengths and angles.

Discussion

Preparation of Low-Valent Osmium Imido Complexes. The easily prepared complexes **2–4** represent a subset of metal–imido chemistry that contains few examples.[9] The (fluoroalkyl)imido compounds prepared by Stone[26] and the Cp*IrNR compounds prepared in our laboratory[11] constitute the only low-valent, late-metal complexes of this type. Other osmium imides have been structurally characterized[22,27–30] and isolated,[31–36] but all exist in high oxidation states.

(25) Trogler, W. C. *Acc. Chem. Res.* **1990**, *23*, 426 and references therein.
(26) McGlinchey, M. J.; Stone, F. G. A. *J. Chem. Soc., Chem. Commun.* **1970**, 1265.
(27) Schofield, M. H.; Kee, T. P.; Anhaus, J. T.; Schrock, R. R.; Johnson, K. H.; Davis, W. M. *Inorg. Chem.* **1991**, *30*, 3595.
(28) McGilligan, B. S.; Arnold, J.; Wilkinson, G. W.; Hussain-Bates, B.; Hursthouse, M. B. *J. Chem. Soc., Dalton Trans.* **1990**, 2465.
(29) Griffith, W. P.; McMannus, N. T.; Shapski, A. C.; White, A. D. *Inorg. Chim. Acta* **1985**, *105*, L11.

Table V. Intramolecular Distances (Å) and Angles (deg) for 2b

intramolecular distance		intramolecular angle	
Os–N1	1.977(13)	N1–Os–N4	74.6(5)
Os–N4	1.942(12)	N1–Os–cent[a]	146.6
Os–C1	2.190(16)	N4–Os–cent	138.7
Os–C2	2.224(16)	Os–N1–N2	117.2(10)
Os–C3	2.215(18)	Os–N1–C11	134.9(10)
Os–C4	2.212(17)	Os–N4–N3	120.6(9)
Os–C5	2.254(16)	Os–N4–C15	129.6(10)
Os–C6	2.234(16)		
Os–cent	1.706	N2–N1–C11	107.9(12)
		N1–N2–N3	116.2(13)
N1–N2	1.351(17)	N2–N3–N4	111.1(12)
N2–N3	1.286(16)	N3–N4–C15	109.7(12)
N3–N4	1.365(16)	C2–C1–C6	121.1(15)
N1–C11	1.531(20)	C2–C1–C7	122.9(15)
N4–C15	1.444(19)	C6–C1–C7	116.0(14)
		C1–C2–C3	121.3(16)
C1–C2	1.423(21)	C2–C3–C4	118.1(16)
C1–C6	1.398(21)	C3–C4–C5	118.8(15)
C2–C3	1.412(22)	C3–C4–C10	118.8(15)
C3–C4	1.465(23)	C5–C4–C10	122.1(15)
C4–C5	1.394(21)	C4–C5–C6	122.6(15)
C5–C6	1.445(20)	C1–C6–C5	117.6(14)
C1–C7	1.554(23)	C1–C7–C8	112.3(15)
C4–C10	1.542(24)	C1–C7–C9	107.4(14)
C7–C8	1.543(24)	C8–C7–C9	110.1(15)
C7–C9	1.548(24)	N1–C11–C12	109.5(14)
C11–C12	1.516(23)	N1–C11–C13	108.1(14)
C11–C13	1.542(24)	N1–C11–C14	106.9(13)
C11–C14	1.563(24)	C12–C11–C13	110.8(14)
C15–C16	1.411(23)	C12–C11–C14	109.7(14)
C15–C20	1.372(23)	C13–C11–C14	111.8(15)
C16–C17	1.48(3)	N4–C15–C16	117.9(15)
C17–C18	1.36(3)	N4–C15–C20	117.5(15)
C18–C19	1.42(3)	C16–C15–C20	124.5(17)
C19–C20	1.47(3)	C15–C16–C17	114.5(17)
		C16–C17–C18	122.3(20)
		C17–C18–C19	122.1(21)
		C18–C19–C20	116.6(19)
		C15–C20–C19	120.0(18)

torsion angle		torsion angle	
N1–Os–cent–C1	109.4(9)	N4–Os–cent–C1	–67.0(8)
N1–Os–cent–C2	170.0(9)	N4–Os–cent–C2	–6.4(8)
N1–Os–cent–C3	–130.6(9)	N4–Os–cent–C3	53.0(9)
N1–Os–cent–C4	–69.3(9)	N4–Os–cent–C4	114.3(8)
N1–Os–cent–C5	–10.4(9)	N4–Os–cent–C5	173.2(8)
N1–Os–cent–C6	50.7(9)	N4–Os–cent–C6	–125.7(8)

[a] cent = centroid of the benzene ring.

The reasons for this absence have been examined by looking at the importance of antibonding orbitals,[12] and molecular orbital diagrams have been devised to explain the unsuspected stability of the Cp*IrNR complexes.[11] This scheme also applies to the compounds (η^6-arene)-OsNR described in this paper. The NR ligand acts as a 4-electron donor, thus making complexes **2–4** formally 18-electron complexes with Os–N triple bonds. Complex **2b**, the first structurally characterized monomeric osmium(II) imide, displays a short Os–N distance of 1.737(7) Å in the solid state and a nearly linear Os–N–C angle of 174.1(7)°, which support a bonding description analogous to that proposed for Cp*IrNR.[9,11] Despite the change in osmium oxidation state, the high oxidation state derivatives show similar Os–N distances (1.65–1.74 Å) and Os–N–C angles (164–179°).[22,27–30] A recent study of transition metal imido complexes by ab initio molecular orbital calculations did not include L_3OsNH, but it is isolobal with CpIrNH.[37] Green and co-workers have investigated the complexes L_nMNR (L_nM = (η^6-arene)Os, Cp*Ir) by photoelectron spectroscopy.[38] This effort has drawn bonding analogies between imido and cyclopentadienyl ligands in these late metal systems and shows good agreement with the qualitative MO diagrams published for Cp*IrNR.[11] In contrast to the results with osmium, the analogous CymRu compounds are dimeric.[14]

In *tert*-butyl early-metal and high-valent late-metal imido complexes, the difference in chemical shift between the α and β carbons of the *tert*-butyl groups, $\Delta\delta$, provides a rough estimate of the electron density on the imido nitrogen.[9] This was measured for imides **2**, giving a $\Delta\delta$ of 27.2 for **2a** and 26.8 for **2b**. The iridium complex has a similar value of 29.3[11] while the high oxidation state osmium–imide, O_3OsN-*t*-Bu, has a $\Delta\delta$ of 55.[39] Even with this information it is difficult to make quantitative judgments since few late transition metal, low-valent imido complexes are known for comparison. These late-metal complexes do not seem to follow established trends in reactivity since, for example, complex **2a** does not react with PhCHO, as predicted[9] for imido compounds with $\Delta\delta < 50$.

Mechanism of the Imide/Amine Exchange Reaction. The imide/amine exchange reaction (eq 2) provided a convenient system to investigate this proton transfer reaction with the CymOs fragment. The reaction of **2a** to **3** goes to completion, and no **2a** was observed by ^{1}H NMR spectroscopy when **3** was treated with 6 equiv of H_2N-*t*-Bu. The kinetic results establish a first-order dependence in both **2a** and amine. A proposed mechanism for the reaction is shown in Scheme III. In the first step, $H_2N(2,6\text{-}Me_2C_6H_3)$ forms a donor complex **A** with imide **2a**. It is possible that hydrogen bonding between the N–H and the imide nitrogen plays an important role; the kinetic study does not address this question. The related imido complexes Cp_2ZrNR add donor ligands to make stable adducts that are similar to **A**, and these adducts serve as a model for this step of the reaction.[40] Intermediate **A** can return to free imide and amine or proceed on to bis(amide) intermediate CymOs(NH-*t*-Bu)(NH(2,6-$Me_2C_6H_3$)) (**B**). When the reaction was followed by ^{1}H NMR spectroscopy, none of the intermediates in Scheme III were present in observable amounts. However, we believe that **B** is a reasonable intermediate, since the chelating bis(amide) compound **5** can be isolated. Presumably, the reaction continues rapidly from **B** and is essentially irreversible. The greater basicity of the nitrogen of the alkylamide ligand compared to that of the arylamide presumably is the reason for $k_3 \gg k_{-2}$.

Since **A** is not observed during the course of the reaction, the steady-state assumption can be made with respect to

(30) Nugent, W. A.; Harlow, R. L.; McKinney, R. J. *J. Am. Chem. Soc.* **1979**, *101*, 7265.
(31) Huang, J.-S.; Che, C.-M.; Poon, C.-K. *J. Chem. Soc., Chem. Commun.* **1992**, 161.
(32) Danopoulos, A. A.; Wilkinson, G.; Hussain-Bates, B.; Hursthouse, M. D. *J. Chem. Soc., Dalton Trans.* **1991**, 269.
(33) Che, C.-M.; Lam, M. H.-W.; Mak, T. C. *J. Chem. Soc., Chem. Commun.* **1989**, 1529.
(34) Smeja, J. A.; Gladfelter, W. L. *Inorg. Chem.* **1986**, *25*, 2667.
(35) Patrick, D. W.; Truesdale, L. K.; Biller, S. A.; Sharpless, K. B. *J. Org. Chem.* **1978**, *13*, 2628.
(36) Chatt, J.; Dilworth, J. R. *J. Chem. Soc., Chem. Commun.* **1972**, 549.
(37) Cundari, T. R. *J. Am. Chem. Soc.* **1992**, *114*, 7879.
(38) Glueck, D. S.; Green, J. C.; Michelman, R. I.; Wright, I. N. *Organometallics*, **1992**, *11*, 4221.
(39) Nugent, W. A.; McKinney, R. J.; Kasowski, R. V.; Van-Catledge, F. A. *Inorg. Chim. Acta* **1982**, *65*, L91.
(40) Walsh, P. J.; Hollander, F. J.; Bergman, R. G. *J. Am. Chem. Soc.* **1988**, *110*, 8731.

Scheme III. Proposed Mechanism for Imide/Amine Exchange (Xyl = 2,6-$Me_2C_6H_3$)

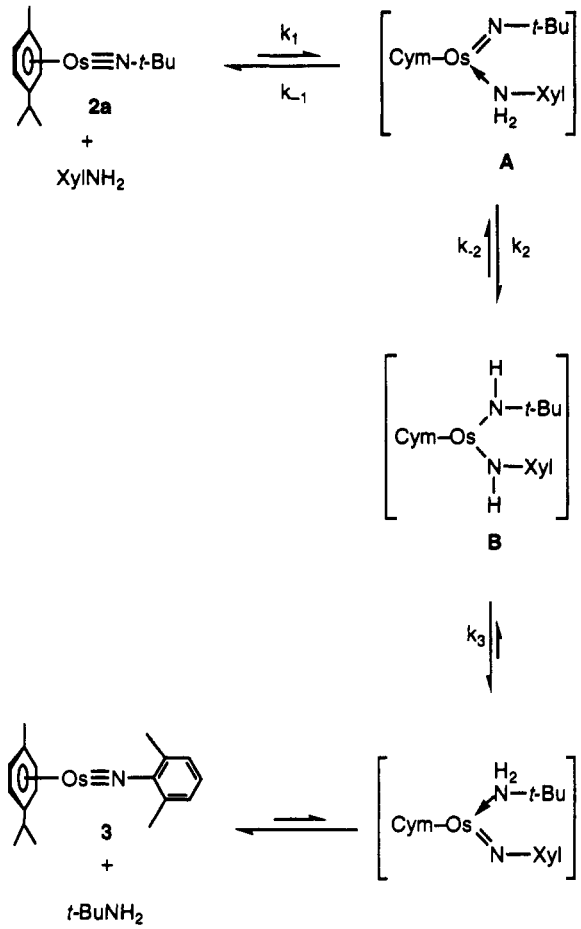

[A]. If we assume $k_3 \gg k_{-2}$, the rate law in eq 4 is obtained.

$$\text{rate} = \frac{d[3]}{dt} = \frac{k_1 k_2 [\mathbf{2a}][H_2N(2,6\text{-}Me_2C_6H_3)]}{k_{-1} + k_2} \quad (4)$$

There are now two possible assumptions that can be made with respect to k_{-1} and k_2. If it is assumed that $k_2 \gg k_{-1}$, the observed rate constant simplifies to eq 5. However,

$$k_{obs} = k_1 \quad (5)$$

the relatively large (primary) deuterium isotope effect is not consistent with this assumption. The rate determining transition state must involve the conversion of **A** to **B** in Scheme III, since the deuterium isotope effect requires that substantial N–H (or N–D) bond breaking must be involved.

If $k_{-1} \gg k_2$ the observed rate constant will simplify to eq 6. This expression is consistent with the observed

$$k_{obs} = \frac{k_1 k_2}{k_{-1}} \quad (6)$$

deuterium isotope effect. Since k_1 and k_{-1} are not involved in the breaking of N–H bonds, they should not be affected significantly by H or D substitution. The deuterium isotope effect (k^H_{obs}/k^D_{obs}) will then simplify as in eq 7.

$$\frac{k^H_{obs}}{k^D_{obs}} \simeq \frac{k^H_2}{k^D_2} = 5.7 \quad (7)$$

We therefore propose that **2a** and $H_2N(2,6\text{-}Me_2C_6H_3)$ are

Scheme IV. Proposed Imide Intermediates in Isocyanate and Azide Reactions with Transition Metals

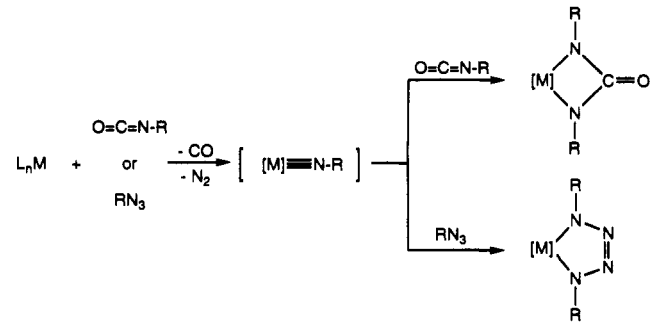

in preequilibrium with **A** and that k_{-1} is large with respect to k_2. The direct, one step conversion of **2a** to **B** cannot be ruled out, but an intermediate like **A** has an analog in the zirconium complexes $Cp_2ZrNR(L)$ mentioned previously.

Complex **5** (Scheme I) offers an interesting structural model for intermediate **B**, since it shows that two primary amides can bond to a CymOs fragment, at least when the groups on the amide are small. This type of compound is also observed in a Cp*Rh complex made from 1,2-diaminobenzene and $[Cp^*RhCl_2]_2$.[41] The formation of **5** rather than the imide $CymOsN[2\text{-}(H_2N)C_6H_3]$ (**C**, Scheme I) suggests that chelation plays an important role. In this situation, enthalpy most likely favors the two σ bonds in **5** to the one σ and one π bond in **C**. Dimerization of **C** would generate a complex similar to the imido dimers of ruthenium $[(\eta^6\text{-arene})RuN(2,6\text{-}Me_2C_6H_3)]_2$,[14,42] which would be apparent by ^1H NMR spectroscopy, but this was not observed. It is also possible that the π-bond in a bent imido ligand, as shown in **C** of Scheme I, is unstable. In the proposed imide/amine exchange scheme, however, an imide and a free amine are entropically more favorable than bis(amide) **B**. But since $\Delta S \approx 0$ for the conversion of **2a** to **3**, $OsN(2,6\text{-}Me_2C_6H_3)$ must be favored by enthalpy over Os-*t*-Bu. A similar exchange mechanism may be involved in the conversion of OsO_4 to O_3OsNR.[43] In contrast, in an early metal imido system, the bis(amide) $Cp_2Zr(NHR)_2$ is thermodynamically favored over the imide $Cp_2Zr{=}NR$ and free amine.[40]

Cycloadditions and Osmium–Nitrogen Bond Formation in Metallacycles. Like Cp*IrN-*t*-Bu, CymOsN-*t*-Bu (**2a**) reacts with a variety of cumulenes (CO, CNR, CO_2). The osmium analogs, though, are not as thermally stable as the iridium compounds, presumably because the neutral *p*-cymene ligand is more easily lost than the anionic pentamethylcyclopentadienyl group.

Late-metal, low-valent imido complexes, similar to **2–4**, have been postulated to be intermediates in the formation of metal urea and tetrazene derivatives (Scheme IV),[23–25] but no direct evidence was obtained for them. The 1,2- or 1,3-dipolar cycloadditions of an isocyanate or azide to an unsaturated metal–nitrogen bond had not been demonstrated, since these metal complexes were unknown. Our isolation of complexes **2** allowed us to explore the possibility of observing cycloaddition reactions between the imido group and organic isocyanates and azides and, thus, demonstrate the chemical properties of the proposed intermediates. The products of these cycloadditions are

(41) Espinet, P.; Baily, P. M.; Maitlis, P. M. *J. Chem. Soc., Dalton Trans.* **1979**, 1542.
(42) Kee, T. P.; Park, L. Y.; Robbins, J.; Schrock, R. R. *J. Chem. Soc., Chem. Commun.* **1991**, 121.
(43) Clifford, A. F.; Kobayashi, C. S. *Inorg. Synth.* **1960**, 207.

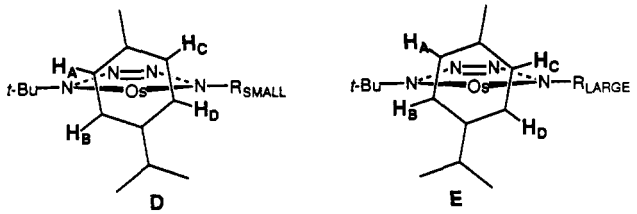

D E

Figure 6. Conformational projections for tetrazene complexes 7–9.

complexes having new metal–nitrogen bonds contained within both four- and five-membered rings.

Direct reactions of the isolated osmium(II) complex **2a** with *t*-BuNCO afforded metallacycle **6** (eq 3). This ureylene complex has many analogs among the transition metals,[44-48] and the $(t\text{-BuN})_2CO$ ligand has been shown to bridge two cobalt atoms,[49] but only two examples are derived from isolated imido complexes.[14,50] This reaction, however, supports the previously held belief that imides may be involved in the metal-catalyzed synthesis of urea derivatives.

Similar cycloaddition reactions were observed by studying the reactions of azides with monomeric imido complexes. Treatment of **2a** with azides RN_3 cleanly provided the tetrazene derivatives (R = Ph (**7**), $SiMe_3$ (**8**), CPh_3 (**9**), and *t*-Bu (**10**)) (Scheme II). This route to these complexes is unique in that it affords both hetero- and homosubstituted ligands. These reactions are believed to proceed because the new ligand can accept electron density into the π^* orbital of the tetraaza skeleton.[25]

The tetrazene complexes display unusual spectroscopic and structural properties, with the size of the substituent introduced with the azide seeming to dictate these features. Broadened lines appear at higher temperatures with larger NR groups (CPh_3 > $SiMe_3$ > Ph) in the ^1H NMR spectra of the heterosubstituted complexes. This variable temperature behavior is consistent with the solid state structural data for **7**, which shows the *p*-cymene ligand tilted toward the phenyl group and away from the more bulky *tert*-butyl group. Projections **D** and **E** of Figure 6 show conformations for small (Ph) and large (CPh_3) substituents. Under these conditions, all four aromatic *p*-cymene protons are in different environments (ABCD). The substituents presumably enforce a lowest energy conformation by hindering the *p*-cymene rotation or slowing a time averaged rocking motion of the *p*-cymene; the larger substituents slow these processes most. The fluxionality in the ^1H NMR spectra is most likely brought on by rotation or rocking around the Os–ring axis. The bis(*tert*-butyl)tetrazene **10** does not display the asymmetry, and the *p*-cymene ligand can lie directly perpendicular to the axis through the osmium and bisecting the tetraaza skeleton (Figure 7).

It has been suggested that resonance structures **F** and **G** contribute to the overall structure of the tetrazene

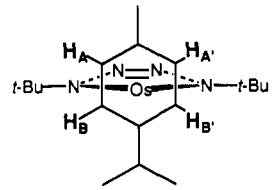

Figure 7. Conformational projection for **10**.

complexes (eq 8).[25] These N_4 adducts are often referred to as metallacyclotetraazapentadienes, but the N–N bond

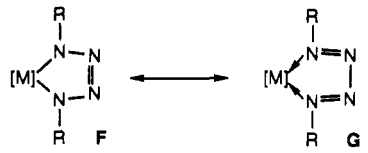

(8)

distances do not support this. The X-ray diffraction data on **7** are most consistent with the valence tautomer **F**, with Os(II) rather than Os(0). The N–N bond lengths are comparable with those in other tetrazene complexes.[25]

The species **7–10** are quite stable but undergo slow thermal decomposition to intractable materials. In contrast to other metal tetrazene complexes, such as the cobalt complex illustrated in eq 9,[51] these osmium compounds

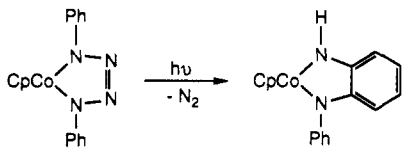

(9)

showed no bond cleavage chemistry upon photochemical excitation or thermolysis. Also, no reactions occurred with Ph_2SiCl_2, Me_3SiI, dimethylacetylenedicarboxylate, CN(2,6-$Me_2C_6H_3$), or PMe_3, suggesting that the system is significantly stabilized by interactions between the metal and the tetrazene ligand π system.

Experimental Section

General Information. Unless otherwise noted, all reactions and manipulations were performed in dry glassware under a nitrogen atmosphere at 20 °C in a Vacuum Atmospheres 553-2 drybox equipped with a MO-40-2 inert gas purifier or using standard Schlenk techniques. The amount of O_2 in the drybox atmosphere was monitored by a Teledyne Model No. 316 trace oxygen analyzer. All ^1H NMR spectra were recorded on either a 200- or 300-MHz Fourier transform instrument constructed at the University of California, Berkeley, NMR facility by Mr. Rudi Nunlist (equipped with Nicolet Model 1280 data collection systems) or Bruker AM-400, AM-500, or AMX-400 spectrometers. $^{13}C\{^1H\}$ NMR spectra were measured at 75.4, 100, or 126 MHz on the various instruments, and assignments were made using standard DEPT pulse sequences. Both ^1H and $^{13}C\{^1H\}$ NMR chemical shifts are reported in parts per million downfield (positive values) from tetramethylsilane. For $^{13}C\{^1H\}$ NMR chemical shift assignments, the *p*-cymene carbon atoms are numbered as follows:[52]

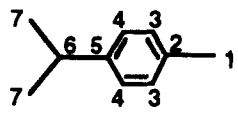

$^{15}N\{^1H\}$ NMR spectra were obtained at 50.6 MHz, and chemical

(44) Herrmann, W. A.; Weichselbaumer, G.; Paciello, R. A.; Fischer, R. A.; Herdtweck, E.; Okuda, J.; Marz, D. W. *Organometallics* **1990**, *9*, 489.
(45) Sahajpal, A.; Robinson, S. D. *Inorg. Chem.* **1979**, *18*, 3572.
(46) Fachinetti, G.; Brian, C.; Floriani, C.; Villa, A. C.; Gustini, C. *J. Chem. Soc., Dalton Trans.* **1979**, 792.
(47) Cenini, S.; Pizzotti, M.; Porta, F.; LaMonica, G. *J. Organomet. Chem.* **1975**, *1975*, 237.
(48) Beck, W.; Rieber, W.; Cenini, S.; Porta, F.; Monica, G. L. *J. Chem. Soc., Dalton Trans.* **1974**, 298.
(49) Matsu-ura, Y.; Yasuoka, N.; Ueki, T.; Kasai, N.; Kakudo, M. *J. Chem. Soc., Chem. Commun.* **1967**, 1122.
(50) Legzdins, P.; Phillips, E. C.; Rettig, S. J.; Trotter, J. C.; Veltheer, J. E.; Yee, V. C. *Organometallics* **1992**, *11*, 3104.
(51) Gross, M. E.; Johnson, C. E.; Maroney, M. J.; Trogler, W. C. *Inorg. Chem.* **1984**, *23*, 2968.
(52) Arthur, T.; Stephenson, T. A. *J. Organomet. Chem.* **1981**, *208*, 369.

shifts are reported in parts per million downfield ($\delta > 0$) from CH_3NO_2. Coupling constants (J) are reported in hertz. Infrared spectra were recorded on a Nicolet 510 Fourier transform spectrometer or a Mattson Galaxy Series FTIR 3000 spectrometer. Elemental analyses were conducted by the University of California, Berkeley, Microanalysis Facility, and mass spectra were recorded by the University of California, Berkeley, Mass Spectrometry laboratory on AEI MS-12 or Kratos MS-50 mass spectrometers. Mass spectral results are reported by the most abundant isotopes (i.e. ^{192}Os), unless reported otherwise.

Benzene, tetrahydrofuran (THF), diethyl ether, and toluene were distilled from sodium–benzophenone. Pentane and hexane were distilled from lithium aluminum hydride. Acetonitrile and methylene chloride were distilled from CaH_2. Compounds $[CymOsCl_2]_2$ (Cym = η^6-*p*-cymene) (**1a**) or $[(\eta^6\text{-}C_6Me_6)OsCl_2]_2$ (**1b**) were prepared by literature methods.[16] Amines H_2N-*t*-Bu, $H_2N(2,6\text{-}Me_2C_6H_3)$, and $H_2N(2,6\text{-}(i\text{-}Pr)_2C_6H_3)$ were stirred over CaH_2 for 24 h and then distilled under reduced pressure before lithiation with *n*-BuLi in toluene. $H_2{}^{15}N(t\text{-}Bu)$ was prepared by a literature method.[11] $1,2\text{-}(H_2N)_2C_6H_3$ was purified by sublimation. $D_2N(2,6\text{-}Me_2C_6H_3)$ for kinetic experiments (>99%) was distilled from CaH_2 and subjected to three freeze–pump–thaw cycles after preparation from $H_2N(2,6\text{-}Me_2C_6H_3)$ and D_2O. *tert*-Butyl isocyanate (*t*-BuNCO) was dried over P_2O_5 and distilled under vacuum. *t*-BuN_3 was prepared as a cyclohexane solution by the method of Pritzkow and Timm,[53] and PhN_3 was prepared by a literature procedure.[54,55] Me_3SiN_3 and Ph_3CN_3 were obtained from Aldrich Chemical Co. and Pfaltz and Bauer, respectively. Unless otherwise noted, all other reagents were used as received from commercial suppliers.

CymOsN-*t*-Bu (2a). THF (50 mL) was degassed using a freeze–pump–thaw cycle under high vacuum and condensed into a flask containing $[CymOsCl_2]_2$ (**1a**) (663 mg, 0.838 mmol), LiNH-*t*-Bu (314 mg, 3.98 mmol), and a stir bar at −196 °C. The solution was allowed to warm to 0 °C and stirred for 1 h at this temperature. The solvent was removed *in vacuo* at 0 °C, and the solid residue was extracted with 50 mL of pentane and filtered. The yellow-brown filtrate was concentrated to half volume under reduced pressure, and 610 mg (1.54 mmol, 92%) of yellow crystals were obtained by cooling this solution at −40 °C. The reaction can be performed at room temperature but diminished yields result (ca. 60%). ^1H NMR (C_6D_6): δ 5.20 (s, 4H, $MeC_6H_4CHMe_2$), 2.42 (sept, J = 6.9, 1H, $MeC_6H_4CHMe_2$), 2.39 (s, 3H, $MeC_6H_4CHMe_2$), 1.37 (1:1:1 multiplet due to coupling with ^{14}N (I = 1), J = 1.5, 9H, $C(CH_3)_3$), 1.29 (d, J = 6.9, 6H, $MeC_6H_4CHMe_2$). $^{13}C\{^1H\}$ NMR (C_6D_6): δ 95.5 (C5), 86.3 (C2), 73.1 (C3 or C4), 69.9 (C3 or C4), 57.1 ($C(CH_3)_3$), 33.1 (C6), 29.9 ($C(CH_3)_3$), 25.2 (C7), 22.3 (C1). Electron impact mass spectrum (EIMS), parent ion envelope: *m/e* (obs *I*, calc *I*) 391 (5.6, 3.8), 392 (5.5, 4.5), 393 (35.8, 32.9), 394 (45.0, 44.2), 395 (72.8, 70.5), 396 (11.6, 10.7), 397 ($[M]^+$, 100, 100), 398 (15.0, 15.9). IR (KBr): 2963 (s), 2944 (s), 2919 (s), 1475 (m), 1354 (m), 1250 (s), 1090 (m), 864 (m), 804 (m) cm^{-1}. Anal. Calcd for $C_{14}H_{23}NOs$: C, 42.51; H, 5.86; N, 3.54. Found: C, 42.64; H, 5.72; N, 3.81.

CymOs^{15}N-*t*-Bu (2a-^{15}N). This compound was prepared by the method used above for **2a** from $[CymOsCl_2]_2$ (**1a**) (92 mg, 0.12 mmol) and $Li^{15}NH$-*t*-Bu (54 mg, 0.68 mmol) in 20 mL of THF. The compound was isolated in 87% yield (80 mg, 0.20 mmol): ^1H NMR (C_6D_6) δ 5.22 (s, 4H, $MeC_6H_4CHMe_2$), 2.43 (sept, J = 6.9, 1H, $MeC_6H_4CHMe_2$), 2.40 (s, 3H, $MeC_6H_4CHMe_2$), 1.36 (d, J = 2.4, 9H, $C(CH_3)_3$), 1.29 (d, J = 6.9, 6H, $MeC_6H_4CHMe_2$); $^{13}C\{^1H\}$ NMR (C_6D_6) δ 95.5 (d, J = 0.8, C5), 86.3 (d, J = 0.8, C2), 73.2 (d, J = 0.8, C3 or C4), 69.9 (d, J = 0.8, C3 or C4), 57.1 (d, J = 0.6, $C(CH_3)_3$), 33.1 (C6), 29.9 (d, J = 0.6, $C(CH_3)_3$), 25.3 (C7), 22.4 (C1); $^{15}N\{^1H\}$ NMR (C_6D_6) δ −64.9; EIMS, parent ion envelope *m/e* (obs *I*, calc *I*) 392 (6.6, 3.8), 393 (6.7, 4.5), 394 (40.1, 32.8), 395 (51.0, 44.0), 396 (80.9, 70.4), 397 (13.9, 10.5), 398 ($[M]^+$, 100, 100), 399 (16.7, 15.5); IR (KBr) 2963 (s), 2943 (s), 2918 (s), 1475 (m), 1354 (m), 1235 (s), 1090 (m), 864 (m), 804 (m) cm^{-1}.

(53) Pritzkow, V. W.; Timm, D. *J. Prakt. Chem.* **1966**, *4*, 178.
(54) Rosen, R. Ph.D. Thesis, University of California at Berkeley, 1990.
(55) Smith, P. A. S. *Org. Synth.* **1951**, *31*, 14.

(C_6Me_6)OsN-*t*-Bu (2b). $[(C_6Me_6)OsCl_2]_2$ (**1b**) (195 mg, 0.230 mmol) and LiNH-*t*-Bu (95 mg, 1.2 mmol) were independently dissolved in THF. The latter solution (4 mL) was added to the solution (13 mL) of **1b** dropwise with stirring at room temperature. The solvent was removed *in vacuo* after 25 min. The residual material was extracted with pentane (10 mL), and this solution was filtered. Removal of the solvent from the filtrate under reduced pressure yielded 190 mg (0.449 mmol, 97%) of yellow **2b**. A sample suitable for microanalysis was obtained by crystallization from heptane: ^1H NMR (C_6D_6) δ 2.37 (s, 18, $C_6(CH_3)_6$), 1.29 (1:1:1 multiplet due to coupling with ^{14}N (I = 1), J = 1.5, 9H, $C(CH_3)_3$); $^{13}C\{^1H\}$ NMR (C_6D_6) δ 82.8 ($C_6(CH_3)_6$), 56.5 ($C(CH_3)_3$), 29.7 ($C(CH_3)_3$), 19.7 ($C_6(CH_3)_6$); IR (KBr) 2971 (s), 2916 (s), 1449 (m), 1378 (m), 1351 (m), 1250 (s), 1066 (w) 1020 (w), 802 (w), 580 (w) cm^{-1}. Anal. Calcd for $C_{16}H_{27}NOs$: C, 45.37; H, 6.42; N, 3.31. Found: C, 45.66; H, 6.43; N, 3.36.

Crystal Structure Determination of 2b. Yellow crystals were obtained by slow cooling of a heptane solution of **2b** to −30 °C for 2 days. A single crystal was mounted in a viscous oil. The crystal used for data collection was then transferred to an Enraf-Nonius CAD-4 diffractometer, centered in the beam, and cooled to −105 °C by a nitrogen flow low-temperature apparatus which had been previously calibrated by a thermocouple placed at the sample position. Automatic peak search and indexing procedures yielded a monoclinic reduced primitive cell. Inspection of the Niggli values revealed no conventional cell of higher symmetry. The final cell parameters and specific data collection parameters are given in Table VI.

The 2185 raw intensity data were converted to structure factor amplitudes and their esd's by correction for scan speed, background, and Lorentz and polarization effects. No decay correction was necessary, but an empirical absorption correction was applied to the data. Space group $C2/c$ was confirmed by refinement. Removal of systematically absent and redundant data left 2076 unique data in the final data set.

The structure was solved by Patterson methods and refined via standard least-squares and Fourier techniques. By deliberate choice only the Os atom was refined with anisotropic thermal parameters. The final residuals for **2b** are given in Table VI.

The quantity minimized by the least-squares program was $\Sigma w(|F_o| - |F_c|)^2$, where w is the weight of a given observation. The *p*-factor used to reduce the weight of intense reflections was set to 0.03 throughout the refinement. The analytical forms of the scattering factor tables for the neutral atoms were used, and all scattering factors were corrected for both the real and imaginary components of anomalous dispersion.

CymOsN(2,6-$Me_2C_6H_3$) (3). Method a. Compound **1a** (90 mg, 0.11 mmol) and $LiNH(2,6\text{-}Me_2C_6H_3)$ (61 mg, 0.48 mmol) were independently dissolved in THF. The amide solution (4 mL) was added to the stirred solution (10 mL) of **1a**. Solvent was removed *in vacuo* after 35 min. The solid residue was dissolved in pentane, the solution was filtered, and the filtrate was exposed to a dynamic vacuum for 12 h in order to remove solvent and free amine. The resulting purple solid weighed 97 mg (0.22 mmol, 96%). A sample suitable for microanalysis was obtained by crystallization from pentane: ^1H NMR (C_6D_6) δ 7.22 (d, J = 7.4, 2H, *m*-$Me_2C_6H_3$), 7.00 (t, J = 7.2, 1H, *p*-$Me_2C_6H_3$), 4.67 (d, J = 5.9, 2H, $MeC_6H_4CHMe_2$), 4.60 (d, J = 5.9, 2H, $MeC_6H_4CHMe_2$), 2.36 (s, 6H, $Me_2C_6H_3$), 2.14 (sept, J = 6.9, 1H, $MeC_6H_4CHMe_2$), 1.87 (s, 3H, $MeC_6H_4CHMe_2$), 0.98 (d, J = 6.9, 6H, $MeC_6H_4CHMe_2$); $^{13}C\{^1H\}$ NMR (C_6D_6) δ 167.6 (*ipso*-C_6H_3), 127.5 (*m*-$Me_2C_6H_3$), 127.3 (*o*-$Me_2C_6H_3$), 121.8 (*p*-$Me_2C_6H_3$), 91.5 (C5), 81.3 (C2), 73.4 (C3 or C4), 70.6 (C3 or C4), 32.5 (C6), 23.9 (C7), 20.2 (C1), 19.6 ($Me_2C_6H_3$); EIMS, a very weak line was

(56) Parameters common to both structures: monochromator, highly-oriented graphite (**2a**, 2θ = 12.0°; **7**, 2θ = 12.2°); detector, crystal scintillation counter, with PHA; 2θ range, 3–45°; background, measured over 0.25($\Delta\theta$) added to each end of the scan for **2a** (0.25($\Delta\omega$) for **7**); intensity standards, measured every hour of X-ray exposure time; unit cell parameters and their esd's were derived by a least-squares fit to the setting angles of the unresolved Mo Kα components of 24 reflections with the given 2θ range. In this and all subsequent tables the esd's of all parameters are given in parentheses, right-justified to the least significant digit(s) of the reported value.

Table VI. Crystal and Data Collection Parameters[56]

	$(C_6Me_6)OsN$-*t*-Bu (**2b**)	CymOs[N(*t*-Bu)-N=NN(Ph)] (**7**)
temp (°C)	−105	−95
empirical formula	$C_{16}H_{27}NOs$	$C_{20}H_{28}N_4Os$
fw	423.60	514.67
cryst size (mm)	0.15 × 0.35 × 0.38	0.11 × 0.30 × 0.43
λ(Mo Kα radiation) (Å)	0.710 73	0.710 73
space group	*C*2/*c*	*Pbca*
a (Å)	13.6502(26)	20.475(3)
b (Å)	13.2523(27)	14.768(2)
c (Å)	18.0151(56)	13.185(3)
α (deg)	90.0	90.0
β (deg)	103.15(20)	90.0
γ (deg)	90.0	90.0
V (Å^3)	3173.4(14)	3983.4(20)
Z	8	8
d_{calc} (g cm^{-3})	1.77	1.72
μ_{calc} (cm^{-1})	80.3	64.2
no. of rflns measd	$+h,+k,\pm l$	$+h,+k,+l$
scan width (deg)	$\Delta\theta = 0.75 + 0.35 \tan\theta$	$\Delta\omega = 0.75 + 0.35 \tan\theta$
scan type	θ–2θ	ω
scan speed ω (deg/min)	5.5	5.49
vertical aperture (mm)	4.0	3.0
horizontal aperture (mm)	2.0 + 1.0 tan θ	2.0 + 1.0 tan θ
setting angles (2θ, deg)	26–30	28–30
no. of rflns collected	2185	2953
no. of unique rflns	2076	2593
no. of obs rflns ($F^2 > 3\sigma F^2$)	1737	1688
T_{max}/T_{min}	0.996/0.604	0.977/0.822
no. of params refined	78	107
$R(F)$ (%)	5.6	4.9
$R_w(F)$ (%)	6.9	5.6
R_{all} (%)	6.7	8.2
goodness of fit	3.11	2.13

observed at *m/e* 889 with no other lines (isotope peaks) around it—it may not be related to the compound; IR (KBr) 2959 (m), 2912 (m), 1458 (m), 1377 (w), 1252 (m), 1220 (s), 1096 (m), 765 (m) cm^{-1}. Anal. Calcd for $C_{18}H_{23}NOs$: C, 48.74; H, 5.23; N, 3.16. Found: C, 48.98; H, 5.12; N, 3.25.

Method b. An NMR tube was charged with **2a** (9.2 mg, 0.023 mmol), hexamethylbenzene (internal standard) (1.3 mg, 0.0080 mmol, 0.35 equiv), and C_6D_6 (0.7 mL). Two, one-pulse ^{1}H NMR spectra were acquired. The *tert*-butyl resonances were integrated vs the methyl groups of the internal standard, and the values from the two spectra were averaged. Under an atmosphere of N_2, $H_2N(2,6\text{-}Me_2C_6H_3)$ (9.6 mg, 0.079 mmol, 3.4 equiv) was added at 25 °C. The solution color changed from yellow to purple within 20 min. The ^{1}H NMR spectra that were obtained after 24 h were identical to that for **3**, as described above, giving a yield of 77%. Within our ability to detect, there was no exchange of bound *p*-cymene with the hexamethylbenzene internal standard throughout the reaction.

CymOsN[2,6-(*i*-Pr)$_2$C$_6$H$_3$] (4). This compound was prepared by the method used to prepare **3** from $[CymOsCl_2]_2$ (**1a**) (91 mg, 0.12 mmol) and LiNH[2,6-(*i*-Pr)$_2$C$_6$H$_3$] (94 mg, 0.51 mmol) in 15 mL of THF. It was isolated in 36% yield (41 mg, 0.082 mmol) by crystallization from CH_3CN: ^{1}H NMR (C_6D_6) δ 7.25 (d, *J* = 7.4, 2H, *m*-$(Me_2CH)_2C_6H_3$), 7.15 (t, *J* = 7.8, 1H, *p*-$(Me_2CH)_2C_6H_3$), 5.11 (d, *J* = 5.5, 2H, $MeC_6H_4CHMe_2$), 4.92 (d, *J* = 5.2, 2H, $MeC_6H_4CHMe_2$), 3.59 (br s, 2H, $(Me_2CH)_2C_6H_3$), 2.52 (sept, *J* = 6.9, 1H, $MeC_6H_4CHMe_2$), 1.92 (s, 3H, $MeC_6H_4CHMe_2$), 1.39 (d, *J* = 6.6, 12H, $(Me_2CH)_2C_6H_3$), 1.03 (d, *J* = 6.9, 6H, $MeC_6H_4CHMe_2$); ^{13}C{^{1}H} NMR (C_6D_6) δ 165.3 (*ipso*-C_6H_3), 138.9 (*o*-$(Me_2CH)_2C_6H_3$), 128.5 (*m*-$(Me_2CH)_2C_6H_3$), 123.1 (*p*-$(Me_2CH)_2C_6H_3$), 93.5 (C5), 82.6 (C2), 72.6 (C3 or C4), 69.4 (C3 or C4), 31.6 (C6), 26.8 ($(Me_2CH)_2C_6H_3$), 26.4 ($(Me_2CH)_2C_6H_3$), 24.2 (C7), 20.2 (C1); IR (KBr) 2959 (s), 2924 (s), 2867 (m), 1459 (m), 1420 (m), 1239 (m), 1189 (s), 794 (w), 773 (w) cm^{-1}. The difficulty in crystallizing **4** away from free amine hindered attempts to obtain satisfactory elemental analysis.

CymOs[1,2-(NH)$_2$C$_6$H$_4$] (5). A benzene solution (3 mL) of 1,2-$(H_2N)_2C_6H_4$ (22 mg, 0.20 mmol) was added dropwise to a stirred benzene solution (12 mL) of **2a** (85 mg, 0.21 mmol). The solvent was removed *in vacuo* after 30 min. The solid was washed with pentane (3 mL), and the residue was dissolved in toluene (5 mL) and filtered through Celite. The filtrate was concentrated to 3 mL and cooled at −40 °C for 12 h, giving 45 mg (0.10 mmol, 52%) of a yellow-orange precipitate that was collected: ^{1}H NMR (C_6D_6) δ 8.68 (br s, 2H, NH), 7.23 (dd, J_1(apparent) = 5.8, J_2(apparent) = 3.3, 2H, C_6H_4), 7.03 (dd, J_1 = 5.9, J_2 = 3.2, 2H, C_6H_4), 5.11 (d, *J* = 5.7, 2H, $MeC_6H_4CHMe_2$), 5.04 (d, *J* = 5.7, 2H, $MeC_6H_4CHMe_2$), 2.11 (sept, *J* = 6.9, 1H, $MeC_6H_4CHMe_2$), 1.95 (s, 3H, $MeC_6H_4CHMe_2$), 1.04 (d, *J* = 6.9, 6H, $MeC_6H_4CHMe_2$); ^{13}C{^{1}H} NMR (C_6D_6) δ 151.8 (*ipso*-C_6H_4), 117.7 (C_6H_4), 113.6 (C_6H_4), 90.6 (C5), 79.8 (C2), 68.1 (C3 or C4), 65.7 (C3 or C4), 32.9 (C6), 24.2 (C7), 21.0 (C1); IR (KBr) 3332 (s, NH), 3065 (w), 2959 (m), 2903 (m), 2868 (m), 1484 (m), 1304 (s), 737 (s), 700 (s) cm^{-1}. Anal. Calcd for $C_{16}H_{20}N_2Os$: C, 44.64; H, 4.68; N, 6.51. Found: C, 44.67; H, 4.64; N, 6.32.

CymOs[1,2-(ND)$_2$C$_6$H$_4$] (5-*d*$_2$). Dinitrogen was bubbled through D_2O for 1 h, and 10 μL (0.5 mmol) of the D_2O was added by syringe to an NMR tube under dinitrogen containing a C_6D_6 solution (0.7 mL) of **5** (4.0 mg, 0.0093 mmol). A ^{1}H NMR spectrum obtained after 12 h was identical to that of **5** except that no resonance was observed at δ 8.68. IR (KBr): 3051 (w), 2959 (m), 2910 (m), 2868 (m), 2474 (m, ND), 1476 (m), 1300 (s), 1033 (m), 730 (s) cm^{-1}.

Kinetics. All kinetics experiments were monitored by ultraviolet–visible spectroscopy using a Hewlett-Packard 8450A instrument equipped with a 89100A temperature controller. Standard solutions were prepared in the drybox in volumetric flasks and stored in the drybox freezer at −40 °C. In a typical run, volumetric pipets were used to deliver 1 ± 0.01 mL of a stock toluene solution of **2a** (2.98×10^{-3} M) and 2 ± 0.01 mL of a stock toluene solution of $H_2N(2,6\text{-}Me_2C_6H_3)$ (1.16×10^{-1} M) to a small vial in the drybox. The concentrations of the species in the reaction solution are listed in Table II. The solution was transferred to a quartz cuvette, which was then sealed with a Kontes high vacuum stopcock, removed from the drybox and placed in the temperature controlled cell holder of the spectrometer. The solution in the cell was stirred with a micro stir bar and a stream of nitrogen was passed through the cell holder to prevent condensation of water onto the cell surface. The temperature of the cell holder was calibrated using a thermocouple which had previously been calibrated using ice and boiling water.

Reactions were monitored by observing the growth in absorbance due to product formation over time. The reactions of CymOsN-*t*-Bu (**2a**) with $H_2N(2,6\text{-}Me_2C_6H_3)$ were observed at 514 nm. In all cases reactions were observed for at least 3 half-lives. Plots of $\ln[A_\infty/(A_\infty - A)]$ vs time gave straight lines with the slope = k_{obs}. These rate constants (Table II) were used in a plot of $[H_2N(2,6\text{-}Me_2C_6H_3)]$ vs k_{obs} (Figure 2), which was also linear. Deuterium isotope effect runs were conducted similarly with $D_2N(2,6\text{-}Me_2C_6H_3)$. The data for these runs are displayed in Table III.

CymOs[(N-*t*-Bu)$_2$CO] (6). A benzene solution (7 mL) of imide **2a** (37 mg, 0.094 mmol) was degassed using a freeze–pump–thaw cycle. Neat *t*-BuNCO (53.8 Torr, 0.192 mmol) was allowed to expand into a bulb of known volume and then condense into the reaction flask at −196 °C. The pressure of the added gas was measured with a MKS Baratron gauge. The solution was heated at 45 °C with stirring for 36 h. Solvent was removed *in vacuo* leaving 45 mg (0.091 mmol, 99%, >99% pure by ^{1}H NMR spectroscopy) of blue-green **3**. Complex **3** sublimed at 60 °C/80 mTorr: ^{1}H NMR (C_6D_6) δ 5.21 (d, *J* = 5.5, 2H, $MeC_6H_4CHMe_2$), 5.15 (d, *J* = 5.5, 2H, $MeC_6H_4CHMe_2$), 2.04 (sept, *J* = 6.9, 1H, $MeC_6H_4CHMe_2$), 1.85 (s, 3H, $MeC_6H_4CHMe_2$), 1.52 (s, 18H, $C(CH_3)_3$), 1.11 (d, *J* = 6.9, 6H, $MeC_6H_4CHMe_2$); ^{13}C{^{1}H} NMR (C_6D_6) δ 174.4 (CO), 87.3 (C5), 76.6 (C2), 73.6 (C3 or C4), 71.2

(C3 or C4), 55.8 ($C(CH_3)_3$), 32.2 ($C(CH_3)_3$), 29.7 (C6), 24.1 (C7), 21.5 (C1); EIMS parent ion envelope *m/e* (obs *I*, calc *I*) 492 (33.0, 32.8), 493 (46.2, 45.7), 494 (72.1, 72.6), 495 (15.7, 14.9), 496 ($[M]^+$, 100, 100), 497 (21.8, 21.7); IR (KBr) 2963 (s), 2921 (s), 1656 (s), 1561 (m), 1450 (m), 1353 (m), 1237 (s), 942 (w), 862 (w), 773 (w) cm^{-1}. Anal. Calcd for $C_{19}H_{32}N_2OOs$: C, 46.13; H, 6.52; N, 5.66. Found: C, 45.82; H, 6.44; N, 5.68.

CymOs[N(*t*-Bu)N=NN(Ph)] (7). A benzene solution (3 mL) of PhN_3 (36.0 mg, 0.302 mmol) was added to a stirred solution of **2a** (91.5 mg, 0.231 mmol) in benzene (7 mL). Stirring was continued for 1 h, and the solvent was lyophilized *in vacuo*. The residue was extracted into pentane and filtered through Celite. The filtrate was cooled at −40 °C for 12 h, at which time 88.5 mg (0.172 mmol, 74%) of a yellow-brown precipitate was collected: ^1H NMR (C_6D_6) δ 7.46 (dd, J_1(apparent) = 8.5, J_2(apparent) = 1.3, 2H, *o*-Ph), 7.17 (m, J = 7.4, 2H, *m*-Ph), 7.14 (tt, J_1(apparent) = 7.4, J_2(apparent) = 1.3, *p*-Ph), 4.90 (d, J = 6.0, 2H, $MeC_6H_4CHMe_2$), 4.86 (d, J = 5.9, 2H, $MeC_6H_4CHMe_2$), 1.95 (sept, J = 6.9, 1H, $MeC_6H_4CHMe_2$), 1.88 (s, 3H, $MeC_6H_4CHMe_2$), 1.78 (s, 9H, CMe_3), 0.82 (d, J = 6.9, 6H, $MeC_6H_4CHMe_2$); $^{13}C\{^1H\}$ NMR (C_6D_6) δ 158.1 (*ipso*-Ph), 128.2 (Ph, verified by DEPT135), 126.0 (Ph), 125.7 (*p*-Ph), 93.8 (C5), 83.2 (C2), 73.1 (C3 or C4), 70.9 (C3 or C4), 67.4 (CMe_3), 33.1 (CMe_3), 32.7 (C6), 24.2 (C7), 21.1 (C1); IR (KBr) 2960 (m), 2918 (s), 2868 (w), 2849 (m), 1593 (m), 1485 (m), 1473 (m), 1450 (m), 1358 (m), 1201 (m), 767 (m), 742 (s), 698 (m) cm^{-1}. Anal. Calcd for $C_{20}H_{28}N_4Os$: C, 46.67; H, 5.48; N, 10.89. Found: C, 46.80; H, 5.45; N, 10.81.

Crystal Structure Determination of CymOs[N(*t*-Bu)N=NN(Ph)] (7). Yellow crystals of **7** were obtained from a concentrated pentane solution cooled to −40 °C. A single crystal was mounted in Paratone N. The crystal was then transferred to an Enraf-Nonius CAD-4 diffractometer, centered in the beam, and cooled by a nitrogen flow low temperature apparatus. The final cell parameters and specific data collection parameters are given in Table VI. The 2953 raw intensity data were converted to structure factor amplitudes and their esd's by correction for scan speed, background, and Lorentz and polarization effects. Inspection of the intensity standards revealed a reduction of 1.6% of the original intensity. The data were corrected for this decay. Space group *Pbca* was confirmed by refinement. The structure was solved by Patterson methods and refined via standard least-squares and Fourier techniques. By deliberate choice only the Os atom was refined with anisotropic thermal parameters. The final residuals for **7** are given in Table VI. Minimization was carried out as for **2b**.

CymOs[N(*t*-Bu)N=NN(SiMe$_3$)] (8). A benzene solution (5 mL) of Me_3SiN_3 (77.2 mg, 0.670 mmol) was added to a stirred solution of **2a** (128 mg, 0.323 mmol) in benzene (15 mL). Stirring was continued for 34 h, and the solvent was then lyophilized *in vacuo*. The residue was extracted into $(Me_3Si)_2O$ and loaded onto a column of alumina III (7 cm × 0.6 cm). After the column was washed with $(Me_3Si)_2O$ (2 mL), the product was eluted with toluene. The solvent was removed from the toluene eluate under reduced pressure leaving 38.3 mg of yellow solid (0.0750 mmol, 23.2%): ^1H NMR (C_6D_6, 22 °C) δ 5.21 (br d, J = 4.2, 2H, $MeC_6H_4CHMe_2$), 5.17 (br d, J = 5.2, 2H, $MeC_6H_4CHMe_2$), 2.03 (sept, J = 6.8, 1H, $MeC_6H_4CHMe_2$), 1.87 (s, 3H, $MeC_6H_4CHMe_2$), 1.75 (s, 9H, CMe_3), 0.90 (d, J = 6.9, 6H, $MeC_6H_4CHMe_2$), 0.52 (s, 9H, $SiMe_3$); $^{13}C\{^1H\}$ NMR (C_6D_6, 22 °C) δ 94.2 (C5), 82.2 (C2), 67.5 (CMe_3), 33.2 (CMe_3), 32.9 (C6), 24.6 (C7), 21.6 (C1), 2.7 ($SiMe_3$); ^1H NMR (toluene-d_8, −58.1 °C) δ 5.10 (d, J = 5.5, 1H, $MeC_6H_4CHMe_2$), 5.00 (d, J = 5.5, 1H, $MeC_6H_4CHMe_2$), 4.97 (d, J = 5.7, 1H, $MeC_6H_4CHMe_2$), 4.94 (d, J = 5.7, 1H, $MeC_6H_4CHMe_2$), 1.94 (sept, J = 6.9, 1H, $MeC_6H_4CHMe_2$), 1.82 (s, 3H, $MeC_6H_4CHMe_2$), 1.77 (s, 9H, CMe_3), 0.91 (t,[57] 6H, $MeC_6H_4CHMe_2$), 0.54 (s, 9H, $SiMe_3$); $^{13}C\{^1H\}$ NMR (toluene-d_8, −58.2 °C) δ 93.4 (C5), 81.9 (C2), 73.5 (C3 or C4), 71.2 (C3 or C4), 69.7 (C3 or C4), 67.7 (C3 or C4), 67.2 (CMe_3), 32.9 (CMe_3), 32.7 (C6), 24.4 (C7), 24.3 (C7), 21.4 (C1), 2.4 ($SiMe_3$); IR (KBr) 2962 (s), 2924 (m), 2868 (w), 1243 (s), 1201 (m), 979 (m), 843 (s), 713 (m) cm^{-1}. Anal. Calcd for $C_{17}H_{32}N_4Os$: C, 39.98; H, 6.31; N, 10.97. Found: C, 40.33; H, 6.30; N, 11.03.

CymOs[N(*t*-Bu)N=NN(CPh$_3$)] (9). A benzene solution (1 mL) of Ph_3CN_3 (36.6 mg, 0.128 mmol) was added to a solution of **2a** (44.9 mg, 0.114 mmol) in benzene (4 mL). This solution was degassed using two freeze–pump–thaw cycles and heated at 45 °C for 4 days. The solvent was then lyophilized *in vacuo*. The residue was extracted into Et_2O and filtered through Celite. The filtrate was cooled at −40 °C for 12 h, at which time 33.0 mg (0.0485 mmol, 43%) of a yellow precipitate was collected: ^1H NMR (C_6D_6) δ 7.49 (m, 6H, *o*-Ph), 7.04–6.99 (m, 9H, *m*/*p*-Ph), 5.18 (br s, 1H, $MeC_6H_4CHMe_2$), 5.13 (br s, 1H, $MeC_6H_4CHMe_2$), 3.96 (br d, J = 4.3, 1H, $MeC_6H_4CHMe_2$), 3.44 (br d, J = 5.2, 1H, $MeC_6H_4CHMe_2$), 2.03 (sept, J = 6.9, 1H, $MeC_6H_4CHMe_2$), 1.79 (s, 9H, CMe_3), 1.77 (s, 3H, $MeC_6H_4CHMe_2$), 0.99 (br d, J = 6.3, 3H, $MeC_6H_4CHMe_2$), 0.94 (br d, J = 6.3, 3H, $MeC_6H_4CHMe_2$); $^{13}C\{^1H\}$ NMR (C_6D_6) δ 147.6 (*ipso*-Ph), 132.3 (Ph), 126.9 (Ph), 126.2 (*p*-Ph), 95.5 (CPh_3), 86.2 (C5), 82.9 (C2), 74.0 (C3 or C4), 73.3 (C3 or C4), 72.5 (C3 or C4), 68.6 (CMe_3), 67.8 (C3 or C4), 33.1 (CMe_3), 30.9 (C6), 25.1 (C7), 23.3 (C7), 20.2 (C1); IR (KBr) 3059 (w), 2966 (s), 2924 (m), 2868 (w), 1595 (w), 1578 (w), 1491 (m), 1475 (m), 1444 (s), 1189 (m), 866 (m), 756 (m), 746 (s), 704 (s), 679 (s) cm^{-1}. High resolution fast atom bombardment mass spectrum (HRFABMS) calcd for $C_{33}H_{39}N_4{}^{188}Os$ (MH^+): 679.273323. Found: 679.271300. The thermal sensitivity of **9** has prevented successful elemental analysis.

CymOs[N(*t*-Bu)N=NN(*t*-Bu)] (10). A cyclohexane solution (0.2 mL) of *t*-BuN_3 (5.88% solution, 0.123 mmol) was added to a stirred solution of **2a** (27 mg, 0.68 mmol) in benzene (7 mL). The solution was filtered through Celite after 4 days of stirring, and the solvent was then lyophilized *in vacuo*. The residue was extracted into pentane and loaded onto a silica column (5 cm × 0.6 cm). A yellow band was eluted with Et_2O (2 mL). The solvent was removed from the Et_2O fraction under reduced pressure leaving 24.4 mg of yellow solid (0.0493 mmol, 72%): ^1H NMR (C_6D_6) δ 5.14 (d, J = 5.7, 2H, $MeC_6H_4CHMe_2$), 5.09 (d, J = 5.8, 2H, $MeC_6H_4CHMe_2$), 2.10 (sept, J = 7.1, 1H, $MeC_6H_4CHMe_2$), 1.94 (s, 3H, $MeC_6H_4CHMe_2$), 1.72 (s, 18H, CMe_3), 0.94 (d, J = 6.9, 6H, $MeC_6H_4CHMe_2$); $^{13}C\{^1H\}$ NMR (C_6D_6) δ 94.4 (C5), 82.5 (C2), 72.5 (C3 or C4), 70.3 (C3 or C4), 68.1 (CMe_3), 33.0 (CMe_3), 32.8 (C6), 24.7 (C7), 21.4 (C1); IR (KBr) 3005 (w), 2972 (s), 2962 (s), 2926 (s), 2866 (w), 1578 (m), 1473 (m), 1450 (m), 1356 (m), 1203 (s), 862 (m) cm^{-1}. Anal. Calcd for $C_{18}H_{32}N_4Os$: C, 43.70; H, 6.52; N, 11.33. Found: C, 43.77; H, 6.41; N, 11.08.

Acknowledgment. We are grateful for financial support of this work from the National Institute of Health (Grant No. GM-25459) and to Prof. Helmut Werner and Degussa AG for arranging a loan of $OsCl_3 \cdot 3H_2O$. Dr. Graham Ball provided assistance with the 2D NMR experiments. The crystal structure analyses were performed by Dr. F. J. Hollander, staff crystallographer at the UC Berkeley X-ray crystallographic facillity (CHEXRAY).

Supplementary Material Available: Additional structural data for complexes **2b** and **7**, including tables of positional parameters and thermal parameters (2 pages). This material is provided with the archival edition of this journal, available in many libraries. Alternatively, ordering information is given on any current masthead page.

OM9302150

(57) This is observed as a 1:2:1 three line pattern at this temperature. Further cooling did not clearly resolve this into the expected two doublets.